

# Irradiation Effects on Scintillation Timing Counter with Series-connected SiPM Readout

G. Boca<sup>a,b</sup>, P. W. Cattaneo<sup>a</sup>, M. De Gerone<sup>c</sup>, F. Gatti<sup>c,d</sup>, M. Nakao<sup>e</sup>, M. Nishimura<sup>e</sup>, W. Ootani<sup>f</sup>, M. Rossella<sup>a</sup>, Y. Uchiyama<sup>f</sup>,  
M. Usami<sup>e,\*</sup>, K. Yanai<sup>e</sup>

<sup>a</sup>INFN Sezione di Pavia, Via A. Bassi 6, 27100 Pavia, Italy

<sup>b</sup>Dipartimento di Fisica, Università degli Studi di Pavia, Via A. Bassi 6, 27100 Pavia, Italy

<sup>c</sup>INFN Sezione di Genova, Via Dodecaneso 33, 16146 Genova, Italy

<sup>d</sup>Dipartimento di Fisica, Università degli Studi di Genova, Via Dodecaneso 33, 16146 Genova, Italy

<sup>e</sup>Department of Physics, The University of Tokyo, 7-3-1 Hongo, Bunkyo-ku, Tokyo 113-0033, Japan

<sup>f</sup>ICEPP, The University of Tokyo, 7-3-1 Hongo, Bunkyo-ku, Tokyo 113-0033, Japan

arXiv:2005.05027v1 [physics.ins-det] 11 May 2020

## Abstract

We studied the effects of radiation damage to SiPMs on scintillation counters with series-connected SiPM readout, especially focusing on timing measurements. We measured the characteristics and performance of counters composed of a  $120 \times 40 \times 5$  mm<sup>3</sup> scintillator tile read out by six SiPMs from AdvanSiD connected in series, for different combinations of samples with various levels of irradiation. First, six SiPMs were equally irradiated step by step with electrons from <sup>90</sup>Sr sources up to a fluence of  $\Phi_{\text{eq}} \approx 3 \times 10^9$  n<sub>1MeV</sub>/cm<sup>2</sup>. The timing resolution of the counter gradually deteriorated by the increase in dark noise. The deterioration and the dark current were suppressed when the setup was cooled from 30°C to 10°C. Second, we studied the characteristics of series-connected SiPMs with different damage levels using the electron-irradiated samples, as well as neutron-irradiated samples. We observed a position dependence of the signal pulse height, the time response, and the timing resolution in a counter.

**Keywords:** Radiation tolerance, Series connected SiPMs, Timing resolution, Scintillation detector

## Contents

<b>1</b>	<b>Introduction</b>	<b>1</b>
<b>2</b>	<b>Radiation damage to SiPMs and series connection</b>	<b>2</b>
2.1	Radiation damage to silicon sensors . . . . .	2
2.2	Scintillation counter with series-connected SiPMs readout . . . . .	2
<b>3</b>	<b>Experimental Setup</b>	<b>3</b>
3.1	Samples and irradiation . . . . .	3
3.2	Timing measurements . . . . .	3
<b>4</b>	<b>Timing resolution and dark current measurement</b>	<b>4</b>
4.1	Waveforms . . . . .	4
4.2	I-V curves . . . . .	4
4.3	Timing resolution . . . . .	4
<b>5</b>	<b>Series connection of differently damaged SiPMs</b>	<b>4</b>
5.1	Patterns of SiPM combination . . . . .	4
5.2	I-V curves and apparent breakdown voltage shift . . . . .	6
5.3	Bias voltage scan at center . . . . .	6
5.4	Hit position dependence in a counter . . . . .	8
<b>6</b>	<b>Discussion</b>	<b>9</b>

## 7 Conclusions

11

### 1. Introduction

Scintillation detectors read out by Silicon PhotoMultipliers (SiPMs) are used in a wide range of experiments to detect charged particles. Series connection of SiPMs is found to be effective to achieve high timing resolutions [1]. This is because the SiPMs' total capacitance is smaller than that of a single SiPM. This sharpens the output pulse shape and leads to a better timing resolution. Recent scintillation detectors, therefore, often adopt series-connected SiPM readouts. Examples can be found in the pixelated Timing Counter (pTC) in the MEG II experiment [2], the electromagnetic calorimeter in the Mu2e experiment [3], and the TOF detector in the PANDA experiment [4].

Though SiPMs are widely used, it is known that highly energetic charged particles and neutrons damage the silicon bulk of SiPMs and degrade their performance by increasing the dark noise. Many studies on the irradiation effects on SiPMs have been presented (recent studies are summarized in [5]). Nevertheless, a detailed study on its effect on the timing resolution of a scintillation counter read out by series-connected SiPMs has not been conducted yet.

In this work, we tested the effect of radiation damage on a scintillation counter read out by a chain of six series-connected SiPMs, especially focusing on the timing resolution. First,

\*Corresponding author

Email address: usami@icepp.s.u-tokyo.ac.jp (M. Usami)

we used six equally-irradiated SiPMs to examine the effect of dark noise increase. Next, we tested several combinations of differently-damaged SiPMs to study additional impacts on timing measurements. Difference in the damage level among the SiPMs can occur if the hit rate in the scintillation detector depends on the position.

## 2. Radiation damage to SiPMs and series connection

### 2.1. Radiation damage to silicon sensors

A lot of studies have been carried out on the radiation damage to silicon sensors, and a growing number of studies concerning SiPMs are now being performed. In these studies, two types of radiation-induced damage are distinguished: bulk damage and surface damage [5].

The bulk damage is caused by collisions of energetic particles leading to displacement of atoms, i.e. lattice defects. It can be further classified into two types: point defects and cluster defects. The fraction of the two is dependent on the type and the energy of incident particles. Low energy electrons, such as those from  $^{90}\text{Sr}$  sources (endpoint at 2.28 MeV), mainly produce point defects while hadrons such as 1-MeV neutrons produce cluster defects. More energetic electrons with  $O(10\text{ MeV})$  energy produce both types with the fraction of cluster defects increasing with the energy.

The dominant effect of the bulk damage on the macroscopic sensor characteristics is an increase in the bulk dark current (leakage current). Therefore, the damage level is often quantified using the dark current increase (the current-related damage rate). In this paper, we also use it as a measure of damage. In the case of SiPMs, the bulk dark current undergoes multiplication and results in dark counts that are indistinguishable from light-induced counts. The increased dark counts affect timing measurements; that is our main concern.

The effects of bulk damage from hadron irradiation were demonstrated to be proportional to the displacement damage cross-section and equivalent to the classical calculation of the non-ionizing energy loss (NIEL) [6]; thus, the NIEL-scaling hypothesis has been widely used to standardize the damage level caused by the irradiation of different types of particles with various energies. To compare the damage level with other studies, it is therefore useful to express exposures as the 1-MeV neutron equivalent fluence  $\Phi_{\text{eq}}$  defined as the product of the fluence and the NIEL value normalized to that for 1-MeV neutrons. However, the violation of the NIEL scaling has been reported in the case of electron irradiation [6]. This is due to different contributions of the point and cluster defects to macroscopic effects [7]. Modified versions of the NIEL calculation have been proposed (see [8] and references therein). Among them is the “effective NIEL” calculated using molecular dynamics simulations [9], which was demonstrated to show better linearity between the calculated values and the current-related damage rates for 1.5–27 MeV electron irradiation [7]. In this paper, we use the effective NIEL for electron/positron irradiation and the classical one for neutron irradiation.

The surface damage, on the other hand, stems from ionization caused by electro-magnetic particles, generating charges in

dielectric ( $\text{SiO}_2/\text{Si}_3\text{N}_4$ ) parts. This results in an increase in surface dark current. The impact on SiPMs was studied in [10] up to 20 MGy of X-ray, which can only induce the surface damage. The result was that the SiPM performance was hardly affected by X-ray irradiation up to 20 kGy, which is larger than the doses relevant to this study. The contribution of the surface current increase to the total dark current increase is also negligible compared to that of the bulk dark current, and thus, we ignore the effect of surface damage in the discussion in this paper.

### 2.2. Scintillation counter with series-connected SiPMs readout

The series connection of multiple SiPMs shows some characteristic features. When  $n$  SiPMs are connected in series, the total sensor capacitance reduces by a factor of  $n$ , as already mentioned, while the effective charge gain of each SiPM also reduces by the same factor. The voltage needed to apply the same bias voltage to each SiPM as to a single SiPM becomes  $n$  times higher. A common current flows through all the SiPMs and balances the bias voltages among the SiPMs. As in the case of parallel connection, not only the photon statistics but also the dark counts are summed.

Here, we briefly present the pTC in the MEG II experiment because the design of our test scintillation counter is based on the design of a pTC counter.

#### MEG II pTC

The MEG II pTC, dedicated to measuring the timing of positrons from muon decays, is composed of 512 plastic scintillator counters. A single counter is a two-side readout plastic scintillator (BC422) with dimensions of  $120 \times 40(50) \times 5\text{ mm}^3$ ; each side is read out by six SiPMs with  $3 \times 3\text{ mm}^2$  active area connected in series.<sup>1</sup> Each side detects roughly 50–100 photoelectrons, depending on the scintillator light yield and the photo-detection efficiency (PDE) of the SiPMs, achieving 70–90 ps timing resolution with the two-side measurement.

The pTC was operated in pilot runs of the MEG II experiment for a month using the nominal intensity positive muon beam ( $7 \times 10^7\ \mu^+/\text{s}$ ) [11]. During the beam time, an increase in the SiPMs’ currents was observed. By linearly extrapolating the increase to the planned three-year data-taking period, the dark currents, a few  $\mu\text{A}$  before the exposure, are expected to reach  $I_{\text{dark}} \sim 100\ \mu\text{A}$  on average at the operating bias voltages ( $V_{\text{over}} \approx 18\text{ V}$ )<sup>2</sup> at  $30^\circ\text{C}$ . The positron flux was measured by the counters. It depends on the position of the counters; the counters at the highest hit-rate region ( $\sim 100\text{ kHz}$ ) will be exposed to  $\Phi_{e^+} \sim 8 \times 10^{10}\ \text{e}^+/\text{cm}^2$  of  $\sim 50\text{ MeV}$  positrons with an absorbed dose of  $\sim 20\text{ Gy}$  in the three-year run. The total fluence is roughly equivalent to  $\Phi_{\text{eq}} \approx 4 \times 10^9\ \text{n}_{1\text{MeV}}/\text{cm}^2$ . The fluence is not uniform inside a counter. It depends on the distance from the beam axis, and the inner-most SiPM will be exposed to roughly triple the flux compared to that of the outer-most SiPM. Preliminary results on the effects of radiation damage were reported in [12].

<sup>1</sup>ASD-NUV3S-P High Gain from AdvanSiD was adopted for the SiPMs.

<sup>2</sup>It corresponds to  $V_{\text{over}} \approx 3\text{ V}$  per SiPM.

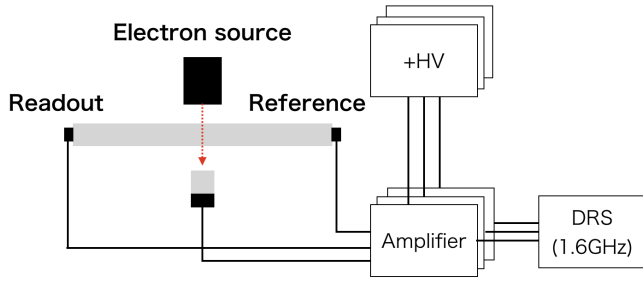


Figure 1: Setup for timing resolution measurements with a scintillator tile read out by the six series-connected SiPMs under test. We set six non-irradiated SiPMs on the opposite side of the tile as reference.

### 3. Experimental Setup

#### 3.1. Samples and irradiation

We prepared SiPM samples (ASD-NUV3S-P High Gain) irradiated with electrons and neutrons. The electron-irradiated samples were mainly used in this study; both in the measurements with equally-damaged SiPMs in Sect. 4 and in the measurements with differently-damaged SiPMs in Sect. 5. The neutron-irradiated samples were used supplementarily in the measurements in Sect. 5.

#### Electron-irradiated samples

We irradiated six SiPMs (#1–#6) to the same dose using two 37-MBq  $^{90}\text{Sr}$  sources. The irradiation was separated into four steps, each 70 hours long. The two sources were swapped alternately between each step to equally irradiate all the samples. During the irradiation, no bias voltage was applied to the SiPMs. Between the steps, the measurement described in Sect. 3.2 was performed. The total fluence in the 280-hour exposure was measured to be  $\Phi_{e^-} \approx 3 \times 10^{12} \text{ e}^-/\text{cm}^2$  with a total dose of 1 kGy, equivalent to  $\Phi_{\text{eq}} \approx 3 \times 10^9 \text{ n}_{1\text{MeV}}/\text{cm}^2$  using the effective NIEL value ( $\Phi_{\text{eq}} \approx 4 \times 10^{10} \text{ n}_{1\text{MeV}}/\text{cm}^2$  using the classical NIEL value).

#### Neutron-irradiated samples

A set of 33 SiPMs was irradiated with neutrons having kinetic energies ranging from 0.5 MeV to 16 MeV using the reactor neutron facilities at the Laboratory of Applied Nuclear Energy (LENA) of the University of Pavia. The set was divided into sub-groups for different fluence levels ranging from  $\Phi_{\text{eq}} \approx 8.7 \times 10^8$  to  $\Phi_{\text{eq}} \approx 5.5 \times 10^{13} \text{ n}_{1\text{MeV}}/\text{cm}^2$ . Among them, two samples with the fluence of  $\Phi_{\text{eq}} \approx 8.7 \times 10^8 \text{ n}_{1\text{MeV}}/\text{cm}^2$  (#7, #8) and two with  $\Phi_{\text{eq}} \approx 5.5 \times 10^9 \text{ n}_{1\text{MeV}}/\text{cm}^2$  (#9, #10) were used in this study.

#### 3.2. Timing measurements

We measured the timing resolution of a counter equipped with the irradiated SiPMs. Figure 1 shows the measurement setup. We used a  $40 \times 120 \times 5 \text{ mm}^3$  scintillator tile (BC422), and the scintillation photons were read out by series-connected SiPM chains. On one end, the SiPMs under test were attached and on the other end, non-irradiated SiPMs were attached as

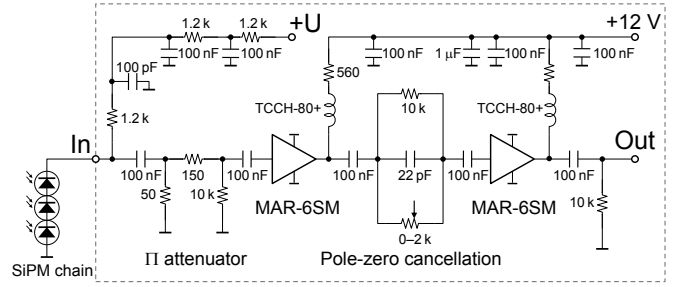


Figure 2: Schematics of the amplifier. The pole-zero cancellation filter can be applied by tuning the adjustable resistor in the circuit [1].

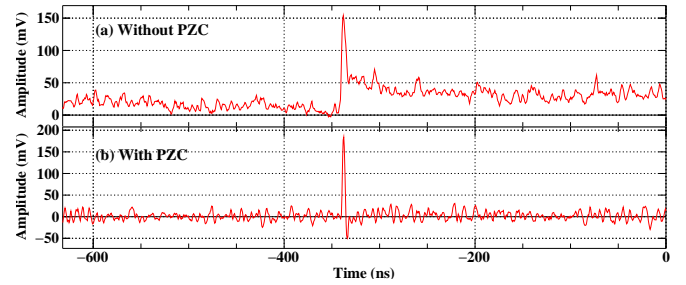


Figure 3: Comparison of typical waveforms with and without the pole-zero cancellation filter (PZC). They are taken with irradiated SiPMs (pattern C in Sect. 5, see the text for the details). The pulse is attenuated to a half with an attenuator in (a).

reference. To align the scintillator tile and the SiPMs, we used a jig produced using a 3D printer. The SiPMs and the scintillator were coupled with optical grease. The electrical contacts with the SiPMs<sup>3</sup> are made by means of spring probe pins so that the series circuit can be made each time without soldering.

Electrons from a 3.7-MBq  $^{90}\text{Sr}$  source were injected to the tile. The trigger signals were generated by a  $5 \times 5 \times 5 \text{ mm}^3$  scintillator (BC422) trigger counter read out by one SiPM (Hamamatsu Photonics S10362-33-050C), located under the scintillator. It has a much better timing resolution ( $\sigma_{\text{trigger}} \sim 30 \text{ ps}$ ) than the test counter [1], and therefore, we used the timing measured by the trigger counter ( $t_{\text{trigger}}$ ) as a reference of the electron hit timing on the test counter ( $t_{\text{signal}}$ ). The time response of the SiPM chain under test was evaluated from the mean value of  $t_{\text{signal}} - t_{\text{trigger}}$  distribution (we call it “time center”) and the timing resolution from its standard deviation.<sup>4</sup>

The output signals were amplified and shaped through a two-staged voltage amplifier with a pole-zero cancellation filter, shown in Fig. 2. The pole-zero cancellation filter realizes a narrower waveform, which is effective for a good timing measurement especially under high dark count rate condition. This is depicted in Fig. 3, which shows typical waveforms after irradiation with and without applying the pole-zero cancellation. The baseline is stabilized by the filter and the dark count effect on the timing measurement is significantly suppressed. The pole-zero cancellation was always activated in this study.

<sup>3</sup>They are surface-mount type.

<sup>4</sup>The counter resolution becomes  $\sqrt{2}$  times better with the two-side readout.

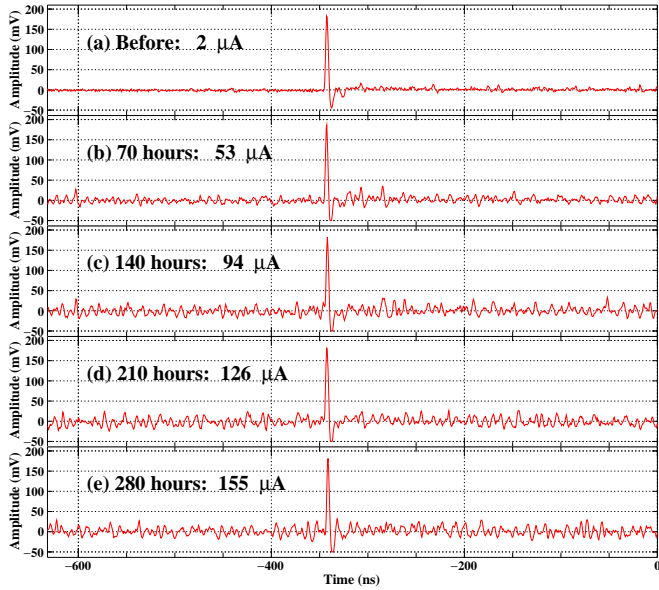


Figure 4: Examples of waveforms at different irradiation steps at 30°C. The applied voltage was set to a fixed value (162.5 V). The dark current values obtained from the I-V curves are also shown.

We recorded the waveform signals using the Domino Ring Sampler chip (DRS4) [13], a waveform digitizer developed at PSI, with the sampling speed of 1.6 GS/s. To pick off the pulse timing, we used the constant fraction method (CFD) with a cubic interpolation between the sampling points.

Some parameters of SiPMs, such as the breakdown voltage and the dark count rate, have significant temperature dependence. Therefore, we performed the measurement at 30°C and 10°C to evaluate the effect of the operating temperature.

## 4. Timing resolution and dark current measurement

### 4.1. Waveforms

Figure 4 shows an example of the waveform from the SiPM chain with the electron-irradiated samples at each irradiation step. The fluctuation of the baseline increased significantly, from an RMS of 2 mV to 10 mV in the four steps, due to the increase in the dark counts.

### 4.2. I-V curves

Figures 5a–e show the I-V curves of each of the six electron-irradiated samples and Figs. 5g–h show the I-V curves when they are connected in series (taken at 0.1 V steps). The dark currents significantly increased by the irradiation; roughly by one order of magnitude below the breakdown and two orders of magnitude above it. On the other hand, the breakdown voltages were only marginally affected by the electron-irradiation damage as shown in Fig. 5f. They were calculated from the maximum point in the second-derivative of the logarithm of the current with three-point smoothing [14] and the systematic uncertainties were estimated from the change by different smoothing.

### 4.3. Timing resolution

We scanned the bias voltage for the best timing resolution in the range 150 – 166 V ( $V_{\text{over}} = 6 - 22$  V), in steps of 2.5 V both at 30°C and 10°C. We first analyzed the data with a fixed CFD fraction of 20% and the results are shown in Fig. 6. The resolution improves with the bias voltage due to a higher gain and PDE, but at some point starts to deteriorate due to increased dark counts. As the fluence increases, the optimal points shift to lower voltages. The timing resolution at each optimal point is gradually worsened and after the fourth irradiation degraded by  $\sim 50\%$ .

Next, we chose three points around each optimal point,  $V_{\text{over}} \approx 11, 13.5, 16$  V for the 30°C datasets and  $\approx 14, 16.5, 19$  V for the 10°C datasets, and optimized the CFD fraction in steps of 10% from 10% to 60% for each dataset. As the noise increases, the optimal fraction value becomes higher: from 20% to 50% in the four steps.

Figure 7 shows the relation between the timing resolution and the dark current. We found that the timing resolution degrades almost linearly with the dark current. When the dark current is increased to  $I_{\text{dark}} \sim 100 \mu\text{A}$ , for example, the timing resolution deteriorates by  $\sim 30\%$  at  $V_{\text{over}} \sim 16$  V.

Compared to the 30°C case, the dark current is significantly lower at 10°C at each irradiation step. Comparing the two cases at  $V_{\text{over}} \sim 16$  V after 140-hour irradiation (the third black marker at 30°C and the second white marker at 10°C in the plot), the dark current decreases from  $I_{\text{dark}} \sim 90 \mu\text{A}$  to  $\sim 20 \mu\text{A}$  and the deterioration of the timing resolution is reduced from 29% to 5%.

## 5. Series connection of differently damaged SiPMs

In the previous section, we examined the relation between the dark noise and the timing resolution of a scintillation counter with equally-damaged series-connected SiPMs. On a more realistic assumption, SiPMs may be irradiated with different doses due to a position dependence of the particle flux. In the following, we show results when differently-damaged SiPMs are connected in series.

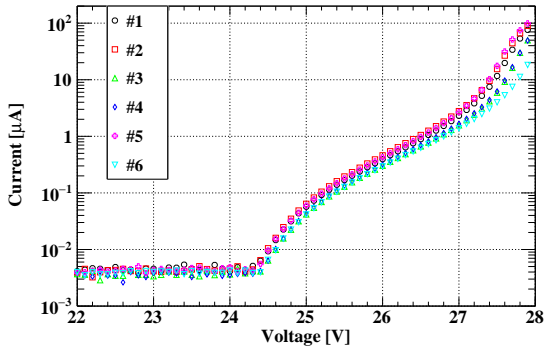
### 5.1. Patterns of SiPM combination

Below we summarize the combinations of SiPMs used for this test:<sup>5</sup>

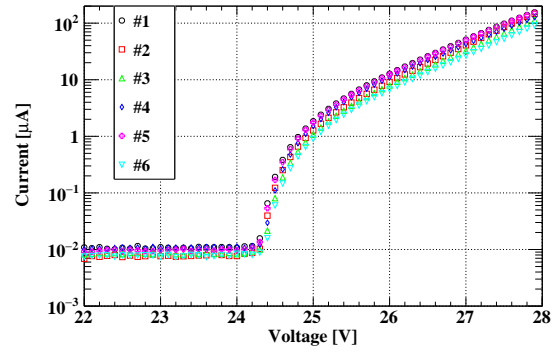
- Pattern A is composed of two electron-irradiated ( $\Phi_{\text{eq}} \approx 3 \times 10^9 \text{ n}_{1\text{MeV}}/\text{cm}^2$ ) SiPMs (#1 and #2 [or #5]<sup>6</sup>) and four non-irradiated SiPMs (#11–#14).
- Pattern B is composed of four electron-irradiated ( $\Phi_{\text{eq}} \approx 3 \times 10^9 \text{ n}_{1\text{MeV}}/\text{cm}^2$ ) SiPMs (#1–#4 [#5]) and two non-irradiated SiPMs (#11, #13).

<sup>5</sup>As mentioned, the radiation damage causes a dark current increase independent of the kind of irradiating particles. Here we distinguish the SiPMs not by the kind of irradiating particles but only by the current level.

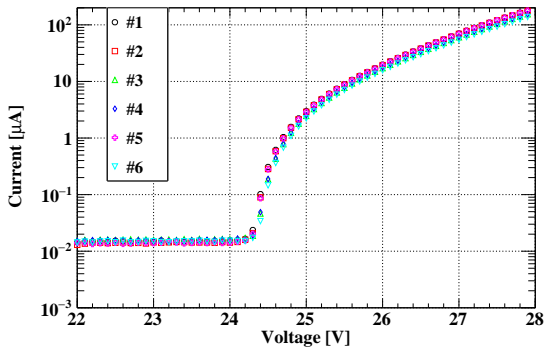
<sup>6</sup>SiPM #2 was broken during the measurement and was replaced with #5, which has the same damage level and I-V characteristics as #2.



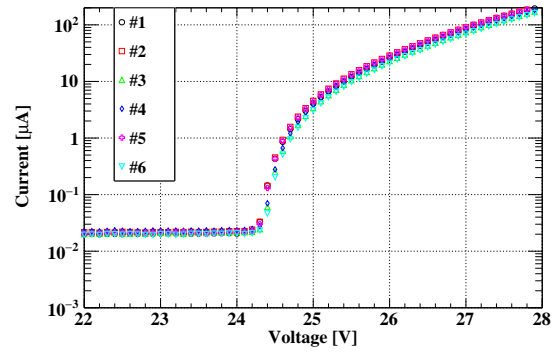
(a) Before irradiation.



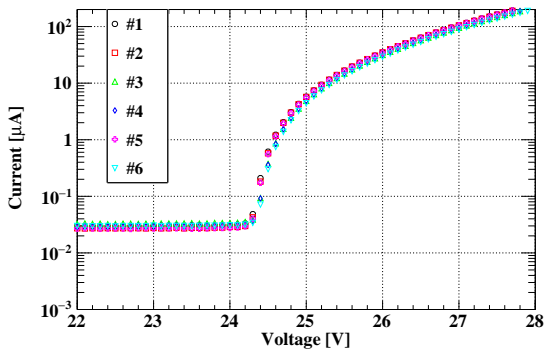
(b) After 70 hours irradiation.



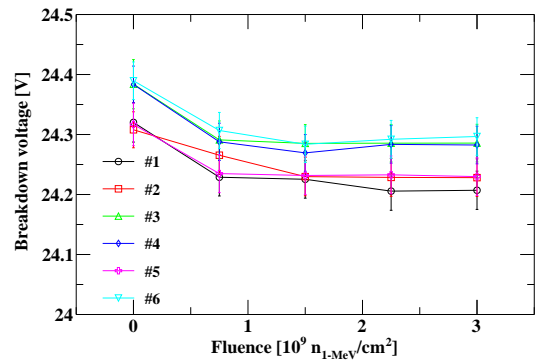
(c) After 140 hours irradiation.



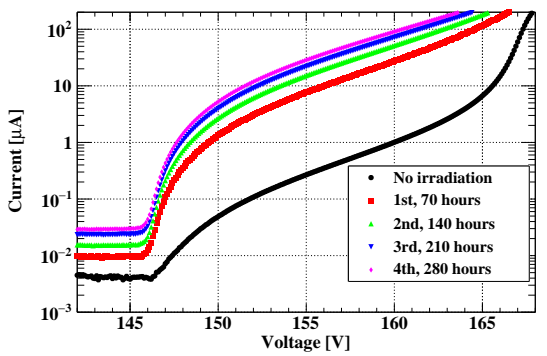
(d) After 210 hours irradiation.



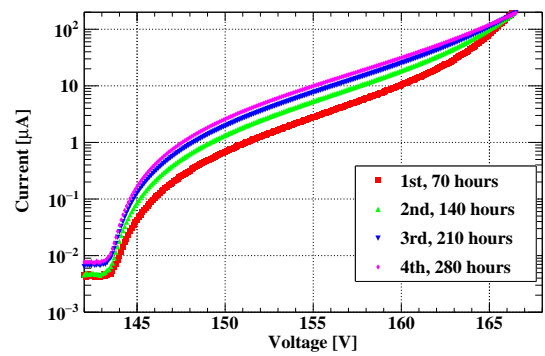
(e) After 280 hours irradiation.



(f) Breakdown voltages of single SiPMs versus fluence.



(g) Six series-connected SiPMs at each irradiation step at 30°C.



(h) Six series-connected SiPMs at each irradiation step at 10°C.

Figure 5: The I-V curves of the six electron-irradiated SiPMs. The I-V data of each SiPM were taken at 30°C (a–e), and the breakdown voltages are plotted in (f). The I-V data of six series-connected SiPMs were taken at 30°C (g) and 10°C (h).

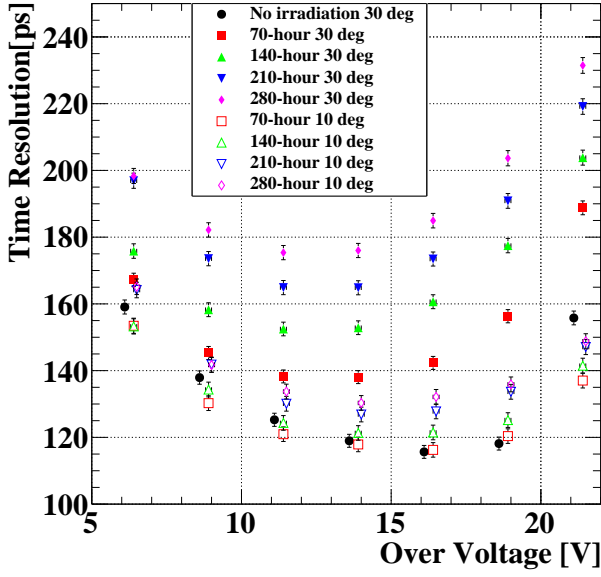


Figure 6: Timing resolution versus over-voltage at 30°C. The CFD fraction was fixed to 20%.

- Pattern C is composed of two electron-irradiated SiPMs (#1, #2 [#5]) and four neutron-irradiated SiPMs, two with the fluence level of  $\Phi_{eq} \approx 8.7 \times 10^8 \text{ n}_{1\text{MeV}}/\text{cm}^2$  samples (#7, #8) and the other two with  $\Phi_{eq} \approx 5.5 \times 10^9 \text{ n}_{1\text{MeV}}/\text{cm}^2$  ones (#9, #10).

Pattern A and pattern B are considered as extreme cases to highlight the effects, while pattern C simulates a gradient damage level closer to a realistic condition.

We define the longitudinal direction of the counter as the  $x$ -axis and the short direction as the  $y$ -axis with the origin point being the center of the scintillator tile. We attached the SiPMs under test to the negative  $x$  side; the signal was extracted from the positive  $y$  side, while the negative  $y$  side was connected to the ground line. We aligned more highly-damaged SiPMs at larger  $y$  position. We call this alignment of SiPMs “normal order”. We also took data with SiPMs aligning in the opposite way in  $y$  direction; we call this “reverse order”. Figure 8 illustrates the alignment of each pattern.

### 5.2. I-V curves and apparent breakdown voltage shift

Figures 9–11 show the I-V curves of individual SiPMs used in the three patterns. Figures 12 and 13 show the I-V curves of them in series measured at 30°C and 10°C, respectively. The breakdown voltages of patterns A and B turned out to be shifted to values higher than that of the all-damaged case (#1–#6).

When the I-V characteristics between series-connected SiPMs differ, the applied voltage to each SiPM is adjusted to accommodate a common current. As a consequence, the over-voltages for the six SiPMs differ from one another; even when the total applied voltage is below the apparent breakdown voltage, voltages applied to non-damaged SiPMs may result to be higher than their breakdown voltages (positive over-voltages)

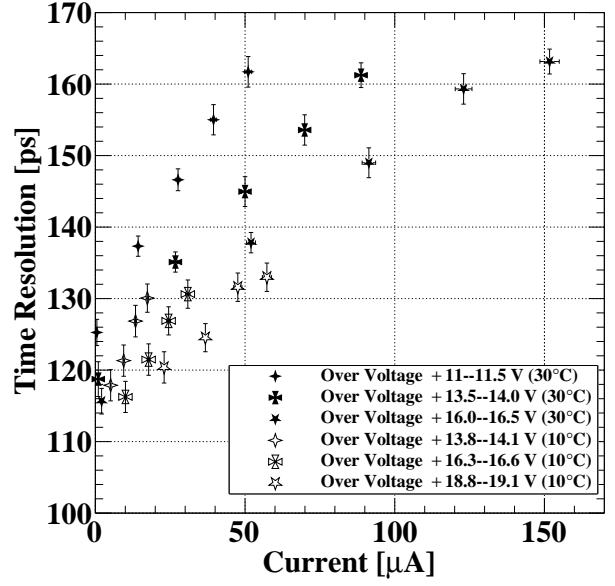


Figure 7: Relation between the dark current and the timing resolution. The CFD fraction was optimized in the range of 10–60%. At the same over-voltage and at the same temperature, the current becomes larger as the irradiation period becomes longer.

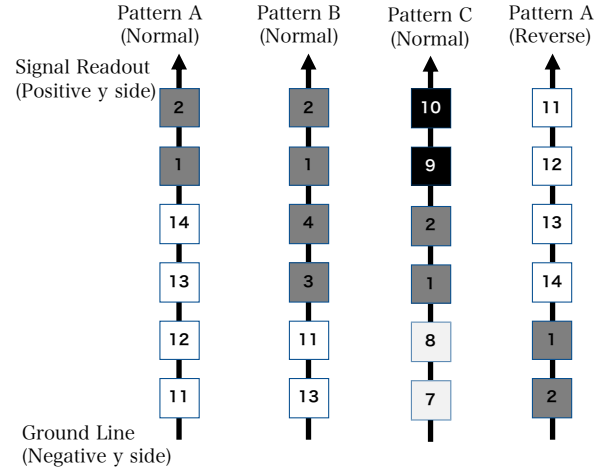


Figure 8: The illustration of SiPM alignment pattern A, pattern B, pattern C in normal order and pattern A in reverse order. SiPMs with higher dark current are shown in black, and those with lower in white.

to allow the same dark current as that of the damaged SiPMs below the breakdown (negative over-voltages). This causes an apparent breakdown voltage shift. Figure 14 depicts this mechanism.

### 5.3. Bias voltage scan at center

First, we took the over-voltage scan data with the measurement setup presented in Sect. 3.2 and evaluated the signal amplitude and the timing resolution. Figures 15 and 16 show the results. Although over-voltages from the apparent breakdown voltages become smaller, the signal amplitudes are the same

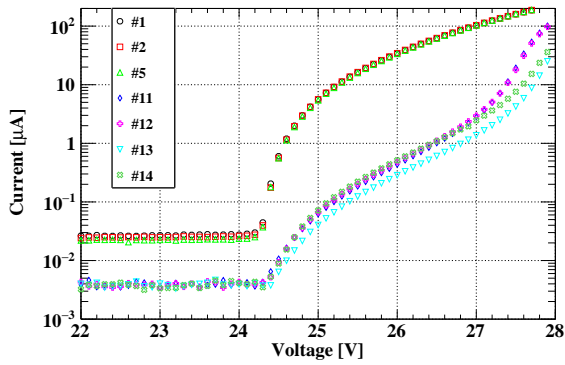


Figure 9: I-V curve of each SiPM used for pattern A.

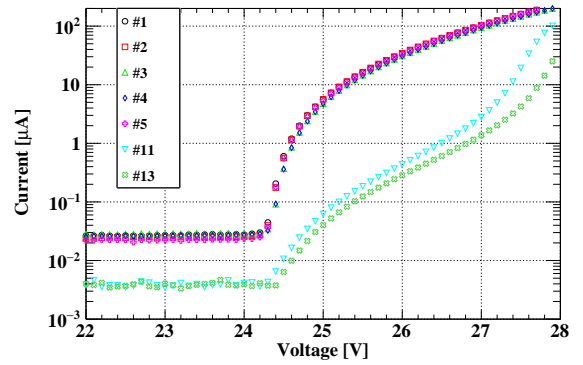


Figure 10: I-V curve of each SiPM used for pattern B.

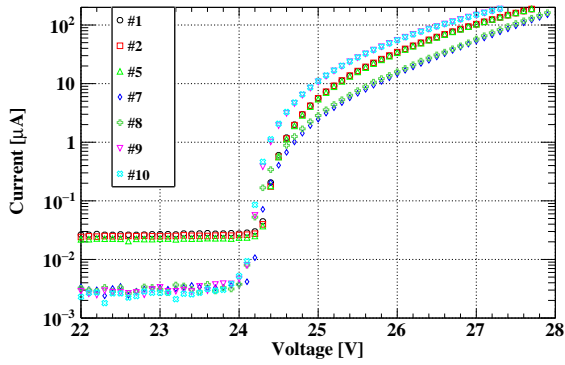


Figure 11: I-V curve of each SiPM used for pattern C.

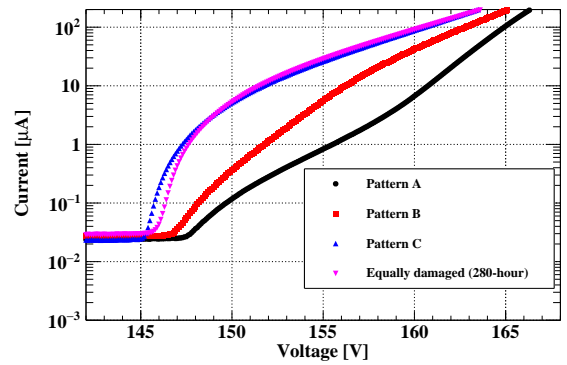


Figure 12: I-V curve of series-connected SiPMs measured at 30°C.

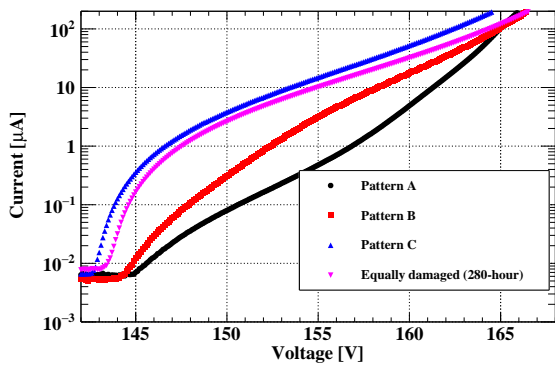


Figure 13: I-V curve of series-connected SiPMs measured at 10°C.

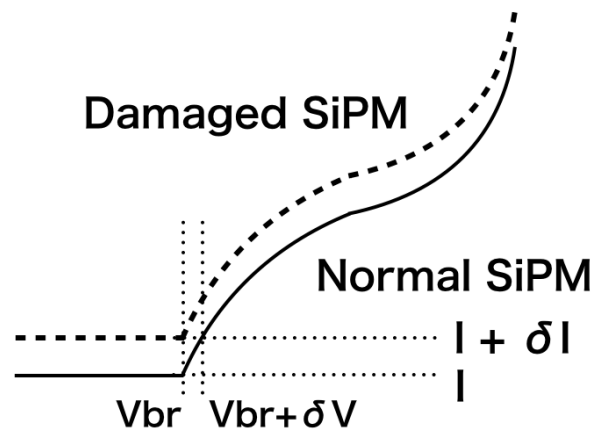


Figure 14: The mechanism of breakdown voltage shift arising from the difference of dark currents. If all the six SiPMs have the same dark current  $I$  at the breakdown voltage  $V_{br}$ , the breakdown voltage of the six-series chain should be  $6 \times V_{br}$ . In pattern A, the breakdown voltage becomes  $6 \times V_{br} + 4 \times \delta V_{br}$ , and in pattern B, it becomes  $6 \times V_{br} + 2 \times \delta V_{br}$  to accommodate the same current  $I + \delta I$  at the breakdown voltage.

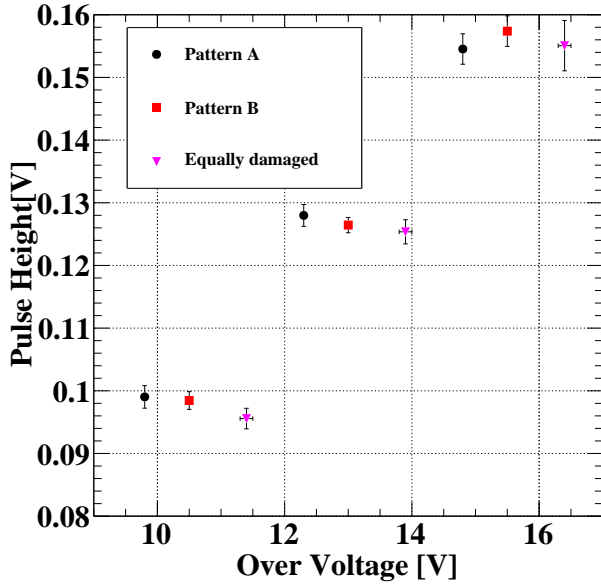


Figure 15: Pulse height at three common voltages (157.5 V, 160.0 V, and 162.5 V) for different SiPM-combinations taken at 30°C. Though the over-voltages from the apparent breakdown voltages are smaller for patterns A and B, the pulse heights are the same in the three configurations. Pattern C is not shown here because the neutron-irradiated SiPMs have different breakdown voltages from the others.

as the all-damaged case; that is, the total effective over-voltage does not change. We also found that no significant change in the timing resolutions compared to the all-damaged case. We can recover the timing resolution again by cooling.

#### 5.4. Hit position dependence in a counter

Next, we examined the dependence of various variables on the hit position in a counter.<sup>7</sup> We took data at different positions in the range of  $-4.25 \leq x \leq 4.25$  cm and  $-1 \leq y \leq 1$  cm in the normal order. Then, we repeated the measurement in the reverse order to clearly distinguish the effect of radiation damage from other effects.

##### Pulse height

Figure 17 shows the dependence of the pulse height on  $y$ -position at  $x = -4.25$  cm. The pulse height is defined here as the most-probable value of its Landau-like distribution. A clear dependence is observed, and the slope is opposite for the normal and the reverse order cases, clearly indicating the effect of the gradient damage to SiPMs. When the illuminated point is close to more-damaged SiPMs the pulse height becomes smaller since the damaged SiPMs, which detect a large fraction of scintillation light in this case, have smaller gain due to the smaller over-voltages.

<sup>7</sup>In this subsection, the pulse height and the noise situation were changed from the measurements in Sect. 4.3 and 5.3 due to a change in the setup. However, we confirmed that those parameters were stable during each measurement, and so the position dependence in different damage patterns can directly be compared.

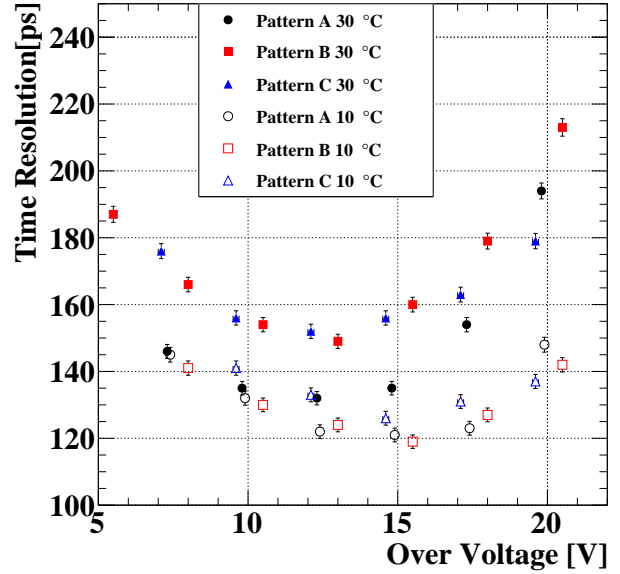


Figure 16: Timing resolution as a function of the over-voltage for the three SiPM-patterns taken at 30°C and 10°C. The CFD fraction was fixed to 20%

When the illuminated point becomes far from the readout channel, the  $y$ -direction dependence of the pulse height is mitigated and at  $x = 0.00$  cm, the dependence becomes almost flat as shown in Fig. 18.

##### Time center

Figures 19 and 20 show the time center at  $x = -4.25$  and 0.00 cm, respectively. Clear and similar  $y$ -dependencies are observed in all the damage patterns at  $x = -4.25$  cm. This time, however, the results of normal- and reverse-order show the same sign of the slope, while the magnitudes of the slope are different. The mechanism yielding the dependence is more complex than that for pulse height because the signal time in the CFD method is determined by multiple factors: the distribution and arrival time of photons to each SiPM, the gain of each SiPM, the time response of each SiPM, and the signal propagation time in the SiPM chain.

The common trend stems from a finite propagation time of the scintillation light in the scintillator and the electronic signal through the SiPM chain. Because of our configuration reading out from  $+y$  side, signals from higher  $y$  hits are detected earlier than those from lower  $y$  hits. This interpretation was confirmed by a measurement using non-irradiated SiPMs.

Deviations from the common trend suggest the effect of the radiation damage but the non-uniform radiation damage complicates matters by the over-voltage variation among the SiPMs, affecting both the gain and the time response. To measure the relationship between the over-voltage and the time response, we measured the over-voltage dependence of the time center for the all-non-damaged case and the all-damaged case. Because of the limited number of non-damaged samples, we performed this measurement using four SiPMs in series. The result is shown



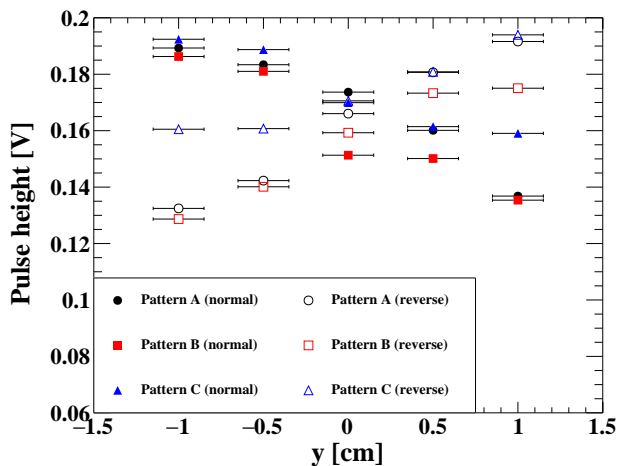


Figure 17: Position dependence of the pulse height in a counter at the nearest point to the SiPMs ( $x = -4.25$  cm). The applied voltage was fixed to 162.5 V at 30°C.

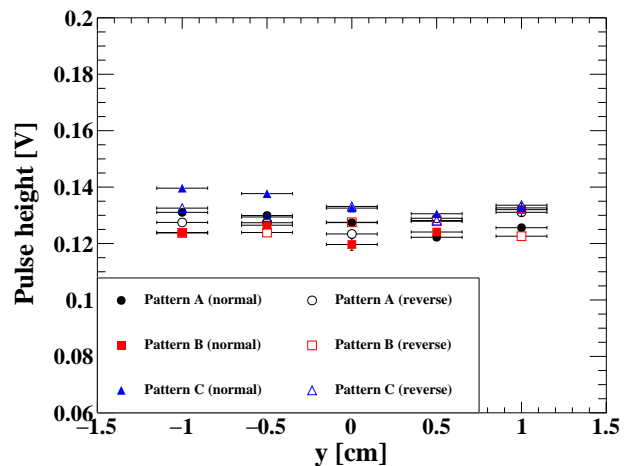


Figure 18: Position dependence of the pulse height in a counter at  $x = 0.00$  cm. The applied voltage was fixed to 162.5 V at 30°C.

in Fig. 21. Both damaged and non-damaged SiPMs show a faster time response with higher over-voltage, although it is saturated at some point. This is due to faster charge collection and avalanche buildup in a stronger electric field. Therefore, SiPMs with less damage in a chain output faster signals than the ones with more damage.

A qualitative explanation for the difference between the normal and the reverse order is as follows. When we measure the timing at the 20% CFD fraction, the leading edge of the pulse is focused on. The main contribution to this part comes from a few SiPMs closest to the signal readout line (i.e.  $+y$  side), especially when the hit point is at higher  $y$ . In the normal order case, these SiPMs yield smaller and slower signals and thus the time center is larger than that in the reverse order case. When the hit point is at lower  $y$ , a smaller fraction of the scintillation light is collected by these SiPMs and signals from successive SiPMs contribute more to the CFD timing. This weakens the effect of the gradient damage. Therefore, similar time center values are obtained in the two cases. As a general trend, the normal order yields less position dependence than the reverse order since the gradient damage effect works to compensate the common trend. The position dependence is mitigated when the fraction of CFD is raised.

When the illuminated point becomes far from the channel, the position dependence in  $y$ -direction becomes gradually smaller.

#### Timing resolution

Figures 22 and 23 show the position dependence of the timing resolution at  $x = -4.25$  and 0.00 cm, respectively. The flipped behavior between the normal and the reverse order cases indicates that the timing resolution predominantly depends on the signal-to-noise ratio. It simply becomes worse when the illuminated point is close to the damaged SiPMs.

The data show slightly better resolutions in the normal order than in the reverse order. This may indicate a second-order effect on the timing resolution from the combination of SiPMs

with different time responses. As discussed in Sect. 5.4, the normal order connection works to compensate the dispersion of signal timings measured by different SiPMs, resulting in a better resolution.

## 6. Discussion

The timing resolution is predominantly determined by the signal-to-noise ratio. Irradiation induces an increase in dark counts and causes deterioration of the timing resolution. We found that the resolution and the dark current are almost in a linear relation. This indicates that we can estimate the resolutions of counters in a running experiment in real time by monitoring the dark currents.

As expected, cooling helps to reduce the impact of the radiation damage on the timing resolution. Because of limitations in the setup, we only tested temperature down to 10°C. Cooling down to lower temperatures will further reduce the impact or enable operation in a harsher environment, although it imposes more constraints, such as thermal insulation and dehumidification, on the detector design. In addition, re-optimization of the operating voltage and the CFD fraction values depending on the damage level turned out to be effective to mitigate the deterioration of the timing resolution.

Annealing of SiPMs can be another way to recover the timing resolution. However, if the SiPMs are glued to the scintillator with optical cement, the applicable temperature is limited to well below 70°C, at which the scintillator melts.

A study on connecting differently-damaged SiPMs in series was performed in [3], in which they measured the charge for laser light read out by three SiPMs connected in series: two of them were non-damaged and one was extensively damaged. We extended it more systematically and quantitatively in this study to find additional effects on the operation and performance of scintillation counters.

We found an apparent breakdown-voltage shift, which is a phenomenon peculiar to the series connection of differently-

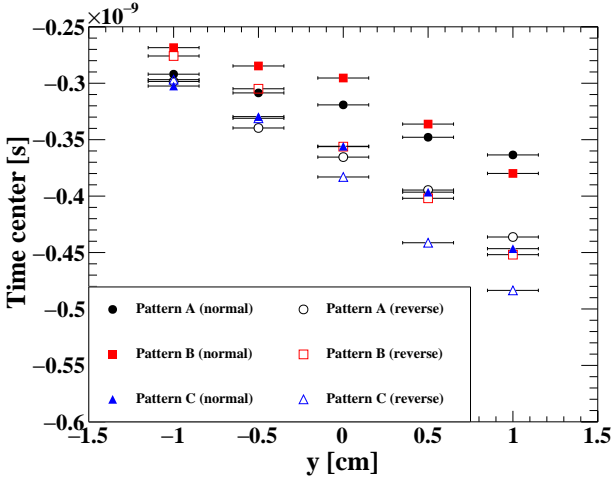


Figure 19: Position dependence of the time center in a counter at  $x = -4.25$  cm. The applied voltage was fixed to 162.5 V at 30°C.

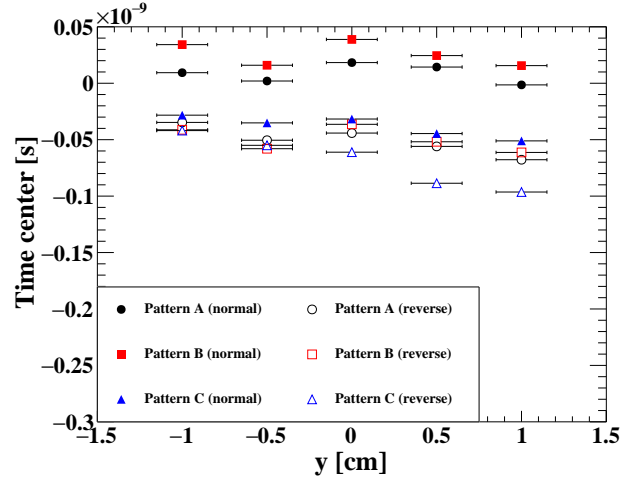


Figure 20: Position dependence of the time center in a counter at  $x = 0.00$  cm. The applied voltage was fixed to 162.5 V at 30°C.

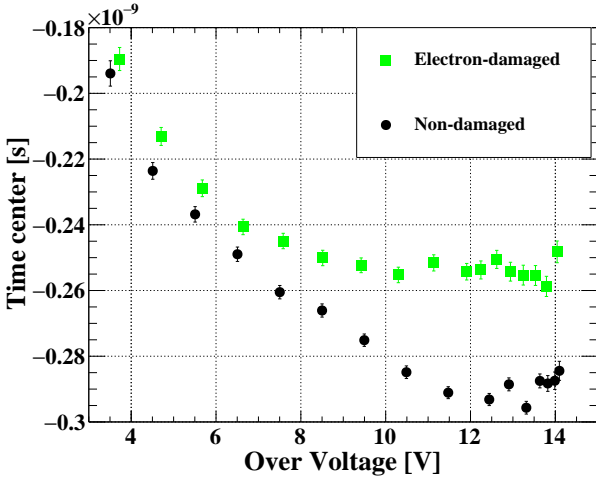


Figure 21: Time center versus over-voltage of four-SiPM chain at 30°C. The non-damaged SiPM chain is composed of #11-#14, and the damaged one is composed of #1, #3-#5.

damaged SiPMs. It spoils the determination of the effective breakdown voltage from the I-V characteristics. Monitoring the operating over-voltage is important for long-term data taking. Therefore, this phenomenon should be kept in mind during the operation of detectors in a real experiment.

As a whole, counters equipped with differently-damaged SiPMs work as properly as those with equally-damaged SiPMs. The pulse height does not change on average and the timing resolution is similar to that of equally-damaged SiPMs with the equivalent damage level. These can be advantageous features of the series connection over parallel connection. In parallel connection, we can keep a fixed over-voltage for each SiPM, leading to the same pulse height. However, in this case, the dark counts are highly non-uniform among the SiPMs, and the operating voltage and the timing resolution can be limited.

A drawback of the series connection we found is the position dependence of the pulse height, the time center, and the timing

resolution, which can be avoided in the case of parallel connection by a careful design of the circuit. The dependence of the pulse height is peculiar to the case with differently-damaged SiPMs, while that of the time center stems from a combination of an intrinsic property of series connection and effects of the different damage levels. The intrinsic one observed in this study is in contrast to the result reported in [1]. The difference could be due to the different sizes of scintillators and different numbers of SiPMs in series.

The variation of the time center in a counter results in a biased time reconstruction depending on the hit position, and thus, this additional spread in the measured time worsens the timing resolution. If the hit position information is available, e.g. from an external tracker, the dependence can be corrected. We found that the dependence changes with different damage levels and the combination of SiPMs. Therefore, the position dependence of the time center should be monitored during an experiment. We also found that the normal order, i.e. extracting signal from the higher damage side, is better because it yields less position dependence than the reverse order. Cooling does not help to reduce the position dependence because the difference of over-voltages between the damaged SiPMs and non-damaged SiPMs does not decrease even when the SiPMs are cooled as shown in Fig. 24.

#### Impact on MEG II pTC

We observed a 41% deterioration of the single-counter timing resolution simply by the increase in dark counts after irradiation of  $\Phi_{\text{eq}} \approx 3 \times 10^9$   $n_{\text{IMeV}}/\text{cm}^2$ , which is equivalent to the average damage level in the MEG II three-year run, at  $V_{\text{over}} \sim 16$  V. This deterioration is suppressed to 13% by cooling the setup to 10°C. The pTC system is equipped with a water chiller system, which can control the detector temperature in the range of 8 – 25°C while it is expected to be  $\sim 30^\circ\text{C}$  without it. The MEG II collaboration adopted 10°C as the operating temperature of the pTC.

The closest approximation to the damage in the pTC chan-

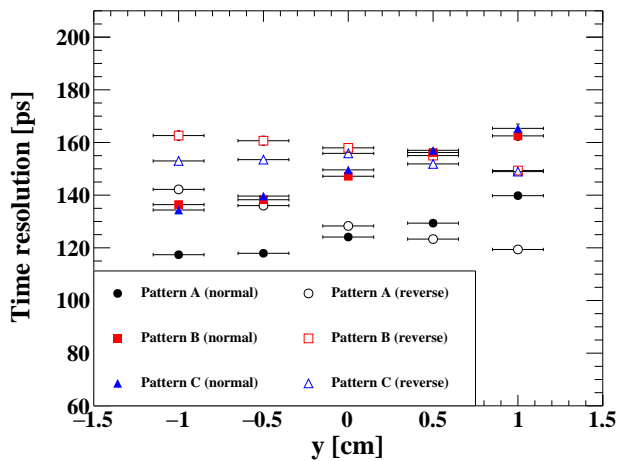


Figure 22: Position dependence of the timing resolution in a counter at  $x = -4.25$  cm. The applied voltage was fixed to 162.5 V at 30°C.

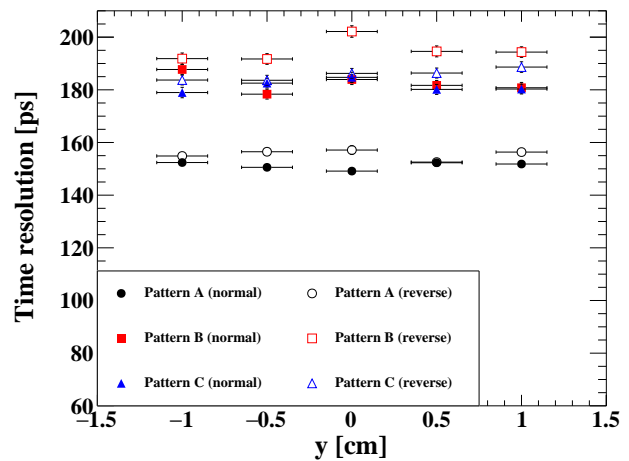


Figure 23: Position dependence of the timing resolution in a counter at  $x = 0.00$  cm. The applied voltage was fixed to 162.5 V at 30°C.

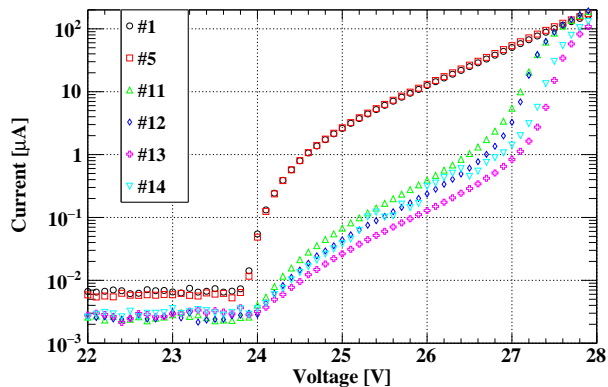


Figure 24: I-V curve of each SiPM used in pattern A at 10°C.

nels is pattern C since the positron flux is larger at smaller radius. Unfortunately, the pTC was designed with the readout from the larger radius side, which corresponds to the reverse order case in this study, and all the counters have been already assembled. A  $y$ -dependence of  $\sim 80$  ps/cm is expected at  $x = -4.25$  cm. An external tracking detector can be used to estimate the hit  $y$ -position. Therefore, a correction for the time center difference can be applied and the deterioration can, at least, be partially compensated.

## 7. Conclusions

We studied the radiation damage effects on a scintillation detector with series-connected SiPM readout. We observed that the dark count increase was the main cause of the timing resolution deterioration. Suppressing the dark counts by cooling the SiPMs effectively recovers the timing resolution. Position dependencies of the pulse height, the time center, and the timing resolution were additionally observed when the SiPMs connected in series have different I-V characteristics. The time center dependence on the hit position can further degrade the

timing resolution. When the damage level has a gradient pattern, the dependence of the time center was found to depend also on the direction of the signal line. We conclude that the signal should be extracted from the higher fluence side. Furthermore, we observed a shift of the apparent breakdown voltage, to which an attention should be paid, because it spoils the determination of the effective breakdown voltage from the I-V curve.

## Acknowledgments

We thank PSI as the host laboratory, and we thank Arnold Marcel from the PSI group who helped us to calculate the source activities. We thank the Laboratorio Energia Applicata LENA in Pavia and in particular Alloni Daniele, Prata Michele, and Salvini Andrea for the irradiation of SiPMs with neutrons. This study was supported by INFN, JSPS KAKENHI Grant Numbers JP26000004, JP19J13635, and JSPS Core-to-Core Program, A. Advanced Research Networks.

## References

- [1] P.W. Cattaneo et al., Development of high precision timing counter based on plastic scintillator with SiPM readout, *IEEE Trans. Nucl. Sci.* 61 (2014) 2657–2666, <https://doi.org/10.1109/TNS.2014.2347576>.
- [2] A.M. Baldini et al., The design of the MEG II experiment, *Eur. Phys. J. C* (2018) 78:380, <https://doi.org/10.1140/epjc/s10052-018-5845-6>.
- [3] N. Atanov et al., The Mu2e calorimeter final technical design report, arXiv:1802.06341
- [4] M. Bhm et al., Fast SiPM readout of the PANDA TOF detector, 2016 *J. Instrum.* 11 C05018, <https://doi.org/10.1088/1748-0221/11/05/c05018>.
- [5] E. Garutti, Yu. Musienko, Radiation damage of SiPMs, *Nucl. Instrum. Methods A* 926 (2019) 69–84, <https://doi.org/10.1016/j.nima.2018.10.191>.
- [6] J.R. Srouf, C.J. Marshall, P.W. Marshall, Review of displacement damage effects in silicon devices, *IEEE Trans. Nucl. Sci.* 50 (2003) 653–670, <https://doi.org/10.1109/TNS.2003.813197>.

- [7] R. Radu, I. Pintilie, L.C. Nistor, E. Fretwurst, G. Lindstroem, L.F. Makarenko, Investigation of point and extended defects in electron irradiated silicon—Dependence on the particle energy, *J. Appl. Phys.* 117 (2015) 164503, <https://doi.org/10.1063/1.4918924>.
- [8] M. Moll, Displacement damage in silicon detectors for high energy physics, *IEEE Trans. Nucl. Sci.* 65 (2018) 1561–1582, <https://doi.org/10.1109/TNS.2018.2819506>.
- [9] C. Inguibert, P. Arnolda, T. Nuns, G. Rolland, “Effective NIEL” in silicon: calculation using molecular dynamics simulation results, *IEEE Trans. Nucl. Sci.* 57 (2010) 1915–1923, <https://doi.org/10.1109/TNS.2010.2049581>.
- [10] C. Xu, R. Klanner, E. Garutti, W.-L. Hellweg, Influence of X-ray irradiation on the properties of the Hamamatsu silicon photomultiplier S10362-11-050C, *Nucl. Instrum. Methods A* 762 (2014) 149–161, <https://doi.org/10.1016/j.nima.2014.05.112>.
- [11] M. Nakao et al., Results from pilot run for MEG II positron timing counter, *Springer Proc. Phys.* 213 (2018) 237–241, <https://doi.org/10.1007/978-981-13-1316-5>.
- [12] M. Usami et al., Radiation damage effect on timing resolution of 6 series-connected SiPMs for MEG II positron Timing Counter, *Nucl. Instrum. Methods A* 936 (2019) 572–573, <https://doi.org/10.1016/j.nima.2018.10.053>.
- [13] S. Ritt, R. Dinapoli, and U. Hartmann, Application of the DRS chip for fast waveform digitizing, *Nucl. Instrum. Methods A*, 623 (2010) 486–488, <https://doi.org/10.1016/j.nima.2010.03.045>.
- [14] M. Simonetta et al., Test and characterisation of SiPMs for the MEGII high resolution Timing Counter, *Nucl. Instrum. Methods A*, 824 (2016) 145–147, <https://doi.org/10.1016/j.nima.2015.11.023>.